Paleocurrent direction measurements in a volcanic setting by means of anisotropy of magnetic susceptibility: A case study from the Lower Miocene Tepoztlán Formation (Transmexican Volcanic Belt, Central Mexico)

Nils Lenhardt[a,*], Harald Böhnel[b], Matthias Hinderer[c], Jens Hornung[c]

[a]Department of Geology, University of Pretoria, Private Bag X20, 0028 Pretoria, South Africa
[b]Centro de Geociencias, Universidad Nacional Autónoma de México, Blvd. Juriquilla No. 3001, 76230 Querétaro, México
[c]Institut für Angewandte Geowissenschaften, Technische Universität Darmstadt, Schnittspahnstraße 9, 64287 Darmstadt, Germany

* Corresponding author: Department of Geology,
University of Pretoria,
Pretoria 0002
South Africa
Tel.: ++27 (0)12 420 3310
Fax: ++27 (0)12 362 5219
E-Mail: nils.lenhardt@up.ac.za

Manuscript published by

Sedimentary Geology

To be sited as:

Lenhardt, N., Böhnel, H., Hinderer, M., Hornung, J., 2013. Paleocurrent direction measurements in a volcanic setting by means of anisotropy of magnetic susceptibility: A case study from the Lower Miocene Tepoztlán Formation (Transmexican Volcanic Belt, Central Mexico). Sedimentary Geology, 290, 1-14.

Abstract

Sources of ancient volcanic rocks are often unknown if they are either eroded and/or covered by younger deposits. This problem, as well as the provenance of reworked volcaniclastic, fluvial and mass-flow deposits, can be partially solved by the application of anisotropy of the magnetic susceptibility (AMS). For massive and poorly sorted volcaniclastic rocks in particular this may be the only way of finding reliable transport directions and therefore allowing for paleogeographic reconstructions. Here, we present a data set of 428 AMS measurements and 249 measurements of sedimentary paleocurrent indicators from the Miocene Tepoztlán Formation at the southern edge of the Transmexican Volcanic Belt (Central Mexico). The highest degree of reliability of AMS measurements is gained for data from lava samples and the lowest from mass flows. Sedimentary structures in sandstones and conglomerates such as trough cross-stratification, asymmetric ripple marks, and the shape of scours and channels could be used to calibrate the results from AMS data and to prove their reliability. AMS data on fluvial deposits point to a drainage system with a W-E flow direction, indicating an outflow of the river system into the ancient Gulf of Mexico.

Keywords: Anisotropy of magnetic susceptibility; paleocurrent direction; volcaniclastic; Transmexican Volcanic Belt; Miocene; Mexico

1. Introduction

In ancient volcanic settings, one challenge in the investigation of volcanic and volcaniclastic deposits is the determination of source vent locations, since former volcanic centers may be either eroded and/or covered by younger deposits. Furthermore, the determination of the provenance of fluvial and mass-flow deposits, arising from the volcanic ring plain itself (Manville et al., 2009, and references therein) or rivers in distal reaches, can also be problematic. In lava flows, both vesicle and crystal preferred orientations have been used extensively for this purpose (e.g., Waters, 1960; Smith and Rhodes, 1972; Walker, 1989; Cashman and Kauahikaua, 1997; Manga, 1998; Iezzi and Ventura, 2002). However, petrological structures such as foliation and lineation due to the movement of a lava flow are often difficult to observe and measure (Bascou et al., 2005). Massive pyroclastic rocks such as ignimbrites and block-and-ash flow deposits rarely show any measurable alignment or structure that can help determine flow direction. However, the magnetic fabric can be used to determine their paleocurrent direction, and the speed, precision, cheapness and range of applicability make it unique in this regard (Tarling and Hrouda, 1993).

All materials, even if they do not acquire remanent magnetization, have a magnetic susceptibility (Liu et al., 2001), which is not always isotropic in the rock (Ising, 1942). This spatial susceptibility variation is defined as the anisotropy of magnetic susceptibility (AMS) and reflects the preferred orientation of magnetic minerals in the rock or sediments, i.e. its magnetic fabric (Hrouda, 1982; Tarling and Hrouda, 1993), which yields three-dimensional flow markers (Cañón-Tapia and Castro, 2004). These can be described as a triaxial ellipsoid within the principal eigenvectors $K_1>K_2>K_3$ representing the maximum, intermediate and minimum susceptibility axes, respectively. The susceptibility depends on the rock's minerals and their relative amounts, and, in the case of primary volcanic rocks, is mainly related to the magma chemistry and crystallization conditions (Zanella et al., 1999). These crystals also determine the susceptibility in the resulting deposits after erosion and redeposition, i.e. in epiclastic fluvial and mass-flow deposits. The AMS gives information on the spatial

arrangement of ferromagnetic (*sensu lato*) and paramagnetic grains, which relates to the emplacement forces. Unlike the natural remanent magnetization (NRM), the AMS components are mainly influenced by relatively coarse particles (Park et al., 2000). This means that the fabric development in sediments is closely related to hydraulic forces. Therefore, the shapes of susceptibility ellipsoids reflect the depositional phase and flow direction during sedimentation (Park et al., 2000).

In lava flows, the fabric is mainly related to the flow conditions and is acquired before complete solidification, at temperatures higher than the Curie or Néel point of ferromagnetic minerals, marking the beginning of remanence acquisition (670 and 575°C, respectively for hematite and magnetite; Zanella et al., 1999). This thermomagnetic remanence is related to the atomic magnetic moments and their interaction in the crystals, and thus completely independent from the regional magnetic fabric. The degree of anisotropy in lava flows is mostly low, the magnetic fabric is mostly planar, and the magnetic foliation is parallel to the flow base (Herrero-Bervera et al., 2002). It is an expected model in lavas that the maximum of the susceptibility axis K_1 (the magnetic lineation) coincides with the flow direction while K_3 (the pole of the magnetic plane) is perpendicular to the surface of the lava flow (Wing-Fatt and Stacey, 1966; Halvorsen, 1974; Kolofikova, 1976). This normal fabric has been observed in many basaltic flows (Herrero-Bervera et al., 2002; Zhu et al., 2003; Bascou et al., 2005). For high shear strains, experimental flow models (Arbaret et al., 1996) show that the elongated particles interact and tend to align at a low angle from the flow direction. Thus, an AMS signature resulting from the imbricate fabric of elongated grains (Cañón-Tapia et al., 1996; Moreira et al., 1999; Geoffroy et al., 2002) should provide valuable information on flow direction.

The behavior of pyroclastic rocks is more complicated, since transportation and deposition dynamics can be highly variable, ranging from concentrated flows which form welded pyroclastic deposits, to dilute, turbulent flows which form surge deposits. Elongate fragments

carried in a pyroclastic density flow may become aligned by the current motion and by interactions with other grains and the substrate, and be preserved in the deposits (Elston and Smith, 1970; Frogatt et al., 1981; LaBerge et al., 2009). The magnetic foliation is commonly inclined with respect to the depositional surface, similar to the imbrication of sediments. The magnetic lineation can be either parallel or perpendicular to flow direction due to rolling or saltation of grains within the flow, and can be misleading in the interpretation of flow direction from magnetic data alone (Ort et al., 2003).

The primary magnetic fabrics of fluvial and mass-flow deposits are predominantly formed during the deposition and arrangement of particles from both traction and suspension in flowing water and thicker viscous fluids (sediment-water mixtures). The initial fabrics are largely determined by gravitational and hydrodynamic forces and, hence, are mainly controlled by the size, shape and mass of detrital grains and velocity of the medium in which they are being transported (Tarling and Hrouda, 1993). In these sediments, the current would usually be parallel to the K_1 axis; in favorable conditions its absolute direction may be inferred from the tilting direction of the K_3 axis (Rees, 1965; Tarling and Hrouda, 1993; Tarling and Shi, 1995; Piper et al., 1996; Abdelayem et al., 1999). However, the current could be perpendicular to K_1 if the flow is strong enough and the grains are fine (Ellwood and Ledbetter, 1977).

The orientation and shape of the AMS fabric has been widely used to determine the orientation of the mineral fabric of rocks and soft-sediments (e.g., Ellwood and Ledbetter, 1979; Lee and Ogawa, 1998; Liu et al., 2001, 2005). The credibility of the AMS fabric as a paleocurrent and depositional indicator is known from work on natural (Ellwood and Ledbetter, 1979; Abdeldayem et al., 1999; Liu et al., 2001) and laboratory deposited sediments (Rees, 1965; Rees and Woodall, 1975). Furthermore, AMS has been used to evaluate flow vectors in lava flows (Cañón-Tapia et al., 1996, 1997; Cañón-Tapia and Walker, 1998; MacDonald et al., 1992) and pyroclastic deposits (e.g., Ellwood, 1982;

Incoronato et al., 1983; Knight et al., 1986; Wolff et al., 1989; MacDonald and Palmer, 1990; Hillhouse and Wells, 1991; Seaman et al., 1991; Ort, 1993; Cagnoli and Tarling, 1997; MacDonald et al., 1998; Ort et al., 1999), in order to determine vent locations, or transport and depositional processes at different distances from the vent (e.g., Fisher et al., 1993; Baer et al., 1997; Le Pennec et al., 1998; Palmer and MacDonald, 1999).

However, several discrepancies have been reported by Bascou et al. (2005): For highly magnetic rocks (such as basaltic lavas) in which AMS is principally carried by ferromagnetic minerals, interpretation of magnetic anisotropy could be complicated by (1) the presence of single-domain magnetic grains with shape anisotropy leading to "inverse susceptibility fabric" (Potter and Stephenson, 1988; Rochette et al., 1992, 1999); (2) interactions between magnetite grains (Stephenson, 1994) due to an anisotropic distribution of ferromagnetic particles (Hargraves et al., 1991); (3) variations of strain in viscous magma (Dragoni et al., 1997); and (4) post-flow alteration or tectonic stresses (Park et al., 1988; Veloso et al., 2007). The interpretation of susceptibility fabrics therefore requires precise information about magnetic mineralogy.

This study attempts a comparison of the quality of AMS data, gained through measurements on three different rocks types (fluvial and volcaniclastic deposits, and lava). We present the results of a combined paleomagnetic, magnetic fabric and sedimentologic study of the Miocene Tepoztlán Formation, Central Mexico, and discuss its implications for the emplacement and source of these deposits.

2. Geological setting

The study area covers approximately 1000 km^2 and is located along the southern edge of the Transmexican Volcanic Belt (TMVB) of Central Mexico, where the Tertiary Tepoztlán

Formation is covered by Quaternary lavas and scoria of the Chichinautzin volcanic field (Márquez et al., 1999; Siebe and Macías, 2004; Siebe et al., 2004). Within this area, the Tepoztlán Formation crops out in an area of 180 km^2 (Fig. 1) and has an overall maximum thickness of 800 m (Lenhardt et al., 2010). The volume of deposited material remaining after erosion was calculated at 130 km^3.

A variety of Eocene–Oligocene (Balsas Group) and older rocks, mostly Cretaceous limestones, underlie the formation. It is covered by lava flows of Pliocene to Holocene age. The Tepoztlán Formation crops out between the San Nicolás Basaltic Andesite and the overlying Basal Mafic Sequence (García-Palomo et al., 2000). The formation of the San Nicolás Basaltic Andesite at 21.6 ± 1.0 Ma (García-Palomo, 1998) suggests deposition contemporaneous with the Tepoztlán Formation (Lenhardt et al., 2010). To the east the Tepoztlán Formation unconformably overlies the Balsas Group and is covered by the Chichinautzin Formation. Magnetostratigraphy combined with K/Ar and Ar/Ar geochronology revealed an Early Miocene age (22.75-18.78 Ma) for the Tepoztlán Formation. The formation can further be subdivided into three units, according to the dominant mode of deposition: (1) the lower fluvial-dominated Malinalco Member (22.8 – 22.2 Ma); (2) the middle eruptive-dominated San Andrés Member (22.2 – 21.3 Ma); and (3) the upper debris-flow-dominated Tepozteco Member (21.3 – 18.8 Ma; Lenhardt et al., 2010).

The Tepoztlán Formation is composed of calc-alkaline volcanic and sedimentary rocks. The volcanic rocks have predominantly andesitic to dacitic compositions, although rhyolites are also present (Lenhardt, 2009). The entire succession comprises pyroclastic (fall, surge and flow deposits), debris-flow and hyperconcentrated-flow deposits, and coarse to fine fluvial and lacustrine deposits (conglomerates, sandstones and mudstones). Only a few lava flows and dikes are present. The Tepoztlán Formation accumulated mainly in medial to distal environments, in flank and apron settings of a volcanic ring plain, which interfingered with an axial W-E trending braided river system (Lenhardt et al., 2011). Subaerial radial ring-plains

usually develop around isolated volcanoes (Palmer, 1991; Palmer and Neall, 1991; Palmer et al., 1993), and consist of resedimented volcanoclastics and occasionally fluvial deposits (e.g., Cas and Wright, 1987; Cronin and Neall, 1997).

Bedding within the Tepoztlán Formation is generally flat-lying or gently dipping at up to 10° to the NNE. This means that the AMS would not have been affected by tectonic shortening. The succession is weakly disrupted by normal faults and sub-volcanic intrusions. Fault displacements are frequently about half a meter and rarely exceed a few meters.

- place **Figure 1** near here -

3. Materials and Methods

Across the study area (1000 km^2), eight stratigraphic sections, ranging in thickness from 78 to 378 m, were logged and sampled for petrographical, sedimentological and paleomagnetic data (Fig. 2). Following the terminology for volcanic and volcaniclastic rocks of McPhie et al. (1993), the sampled rocks can be classified as lava, tuff, tuffaceous breccias, conglomerates and sandstones, originating from different transport and depositional processes during or after volcanic eruptions. A total of 428 samples of lava, tuff, sandstones, and the fine-grained matrix of tuffaceous breccias was drilled with a gasoline-powered tool from 49 sites. Drill cores were not taken from conglomerates due to their coarse grain sizes. However, the conglomerates were used for sedimentological analysis. The number of cores per site depended on outcrop condition, and varied from 5 to 28. One or two cylindrical, 2.2-cm long specimens were cut in the laboratory. The natural remanent magnetization (NRM) and anisotropy of magnetic susceptibility in low fields (300 Am^{-1}) were measured at the Centro de Geociencias, UNAM, Querétaro, Mexico using a JR-5 spinner magnetometer and a KLY-3 susceptibility bridge (AGICO), respectively.

The magnetic susceptibility (K) relates an induced magnetic moment to the inducing magnetic field. The AMS generally reflects the shape of this magnetic moment and the preferred orientation of paramagnetic and ferrimagnetic mineral grains. The maximum (K_1), intermediate (K_2) and minimum (K_3) susceptibility directions for each sample were derived from a set of measurements in 15 different orientations and described by declination and inclination. In order to evaluate the relationship between depositional processes and magnetic fabrics in the rock record of the Tepoztlán Formation, the following AMS parameters were used, following the recommendation of Jelinek (1981), Ellwood et al. (1988), and Tarling and Hrouda (1993):

The *mean magnetic susceptibility* (Nagata, 1961),

$K_m = (K_1+K_2+K_3)/3$ in the SI definition;

the *corrected degree of anisotropy* (Jelinek, 1981),

$P_j = \exp\sqrt{\{2[(\eta_1-\eta_m)^2+(\eta_2-\eta_m)^2+(\eta_3-\eta_m)^2]\}}$, where $\eta_1 = \ln K_1$; $\eta_2 = \ln K_2$; $\eta_3 = \ln K_3$;

$\eta_m = \sqrt[3]{\eta_1 \cdot \eta_2 \cdot \eta_3}$;

the *magnetic lineation* (Balsley and Buddington, 1960),

$L = K_1/K_2$;

and the *magnetic foliation* (Stacey et al., 1960),

$F = K_2/K_3$.

The *ellipticity of the susceptibility ellipsoid* was expressed by the shape parameter T (Jelinek, 1981) defined by: $T = (2\eta_2 - \eta_1 - \eta_3)/(\eta_1 - \eta_3)$ with $T > 0$ for oblate magnetic susceptibility

ellipsoids, and $T < 0$ for prolate magnetic susceptibility ellipsoids. T may vary from -1 (perfectly prolate ellipsoid, $K_{max} > K_{int}$ and K_{min}) to +1 (perfectly oblate ellipsoid, K_{max} and $K_{int} > K_{min}$), while $T = 0$ corresponds to a triaxial ellipsoid. T and P_j are based on logarithmic values, η_1, η_2 and η_3, of K_1, K_2 and K_3, respectively. The shape parameter T is used to identify the magnetic fabric type and to determine the depositional conditions. T values are positive (negative) when magnetic fabrics show magnetic foliation (magnetic lineation) (Jelinek, 1981; Hrouda, 1982). The parameter P_j is used to represent the degree to which the magnetic fabrics are developed internally, with higher values implying a high degree of internal anisotropy (Hrouda, 1982). The magnetic lineation and foliation at sample and site scales are defined as the K_1 direction and the plane normal to K_3, respectively.

AMS fabrics are shown in Fig. 4 and AMS parameters are listed in Table 1. The significance of the magnetic fabric of the studied rocks was tested using the tensorial mean statistics of Jelinek (1978), and calculated by using the ANISOFT program written by Martin Chadima and Vit Jelinek. These statistics provide mean directions for K_1, K_2 and K_3 with ellipses of confidence (α_{95}), together with L, F and the mean tensor.

A key factor in the correct interpretation of the AMS within the Tepoztlán Formation was the comparison of results with other structures that bear a more evident relation to flow direction, such as particle alignment in coarse-grained sediments (e.g., Ellwood, 1982; Incoronato et al., 1983; Capaccioni and Sarocchi, 1996), dip directions of foresets, and linear scour marks (Reineck and Singh, 1980; Allen, 1984; Reading, 1996). The coarseness of the clastic sediments meant that few sedimentary structures could be identified, generally only allowing measurements in sandstones.

- place **Figure 2** near here -

.

4. Results

4.1. Lithology and petrography

The studied samples of the Tepoztlán Formation comprise 5 volcanic and sedimentary lithofacies types distinguished on the basis of rock type, sedimentary and volcanic structures or textures, and grain size, consisting of lava, tuff, tuffaceous breccia, sandstone and conglomerate (Lenhardt et al., 2011).

Lava

The 15-25 m-thick flows within the Tepoztlán Formation commonly have a blocky crust and a dense core, and exhibit an irregular, unconformable contact with the underlying deposits. Angular fragments of the crust range from 3-50 cm in size at the base or the top of massive flows. All flows have a porphyritic to glomeroporphyritic texture. Plagioclase is the most abundant mineral with subordinate K-feldspar, clinopyroxene and amphibole. Accessory minerals consist of mica, abundant titanomagnetite and other accessories (Lenhardt et al., 2010). The groundmass shows a hyalophylitic, sometimes trachytic texture, comprised of plagioclase microlites and an ore phase (titanomagnetite). The whole-rock SiO_2 content of the lavas ranges from 55.9 to 60.6 wt%, identifying them as andesites or dacites (Lenhardt, 2009). The volcanic facies, represented by andesites and dacites, are interpreted as viscous, slow moving blocky lava flows (MacDonald, 1972; Mueller, 1991) as they are associated with lava domes and coulées (Williams and McBirney, 1979; Orton, 1996). The massive to brecciated units display the attributes of a coherent flow in which autobrecciation processes were prevalent and produced breccia during flow advance (Bonnichsen and Kauffmann, 1987).

Tuff

The massive pumice-rich tuffs exhibit accessory and minor lithic fragments (up to 10 cm in diameter) in a matrix of bubble wall shards and phenocrysts (feldspars, augite, rare quartz). Accessory lithic clasts are comprised of gray to red porphyritic rocks of dacitic to andesitic composition (58.5-66.5 vol% SiO_2; Lenhardt, 2009). Pumice clasts range from creamy white to pale yellow in colour. They are relatively dense to finely vesicular and usually porphyritic, containing predominantly augite and plagioclase as phenocrysts. Within the matrix, pumice clasts usually do not exceed diameters of 6 mm. However, in pumice concentration zones on top of single units, clasts can reach up to 10 cm in diameter. Due to transportation and abrasion they appear subrounded to rounded. The deposits usually show a normal coarse-tail grading of the lithic clasts while the pumice clasts show a reverse grading. Thicknesses of single units can vary from 0.1 to 9.0 m with an average of 1.5 m. The deposits partly drape the pre-eruption topography, thickening in valleys and depressions. Their lower bounding surfaces are flat or reflect the paleosurface, whereas their tops are mostly eroded. The deposits occur as single units or as a series of stacked beds.

This lithofacies is interpreted as an ash-flow deposit and analogous facies are described by many authors as the most common ignimbrite lithofacies (e.g., Ross and Smith, 1961; Sparks, 1976; Wilson and Walker, 1982; Branney and Kokelaar, 2002).

Tuffaceous breccia

This lithofacies is composed of angular to subangular clasts in a pinkish red matrix of fine to medium sand. They occur in laterally extensive sheets (up to several hundred meters across) planar bases and eroded tops. Average thickness of single units is about 4 m; however, vertical amalgamation surfaces between stacked units are rarely visible, resulting in deposits up to 14 m thick without any visible bounding surfaces. The deposits show no signs of grading or sorting. Clasts are usually pebbles and cobbles up to 20 cm diameter; however, single outsized clasts up to 2 m diameter have been observed. The matrix of the deposits is

commonly composed of lithic and pumice fragments, crystals of quartz and feldspar and glass shards, showing significant alteration to clay minerals. The fragments do not show any alignment within the matrix.

The poor sorting and massive appearance are evidence for transport and deposition of this lithofacies by and from debris flows (Hampton, 1975; Johnson and Rodine, 1984; Smith and Lowe, 1991; Coussot and Meunier, 1996; Pierson et al., 1996).

Conglomerate

This lithofacies is poorly sorted with grain sizes from fine sand to cobbles. Gravels are dominant are subangular to subrounded and up to 20 cm across. Locally, lenses of cross-stratified sandstone occur. The matrix dominantly consists of sand-sized grains, comprising small clasts of lava, pumice or ash particles. The conglomerates form single beds or sets of stacked beds separated by thin sandy layers. Thicknesses vary from 0.2 to 6 m with an average of 1 m. The conglomerates show flat or concave lower bounding surfaces, pinching out laterally. Lenticular strata are bounded by scour surfaces. Laterally, they extend up to several tens of metres.

This lithofacies is very common in gravel-bedload stream deposits (e.g., Steel and Thompson, 1983; Smith, 1990; Siegenthaler and Huggenberger, 1993) and as sheets and gravel bars in braided river systems (e.g., Miall, 1977).

Sandstone

This lithofacies consists of grey tuffaceous sandstones, comprising glassy material, small lava and pumice particles and minor rounded phenocrysts, dominated by feldspars and pyroxenes. Trough cross-bedding is the dominant sedimentary structure. However, planar cross-bedding or scour-fill bedding is also common. Individual units are stacked, often forming multilateral and single- or multistorey packages. The thicknesses of the units range from 0.1 to 6 m with

an average of 0.8 m. The lateral extent cannot be determined clearly in all cases; however, some outcrops extend up to 150 m. They are characterized by erosive, concave-up to flat bases. Laterally, individual elements pinch out or are completely eroded away. Subangular to subrounded, pebble- to cobble-sized clasts (up to 20 cm) are concentrated along erosional contacts. Fining-upward successions are common, often with clayey, ripple cross-laminated layers on top.

Based on the composition, the presence of crystals and the absence of basement material, the original fragmentation process and components support an initial pyroclastic origin. However, the sedimentary structures indicate significant reworking of either primary pyroclastic material or material that had previously been reworked by lahars. Cross-stratification with a unimodal paleocurrent pattern, fining-upward sequences, and channel scours at the base are all consistent with fluvial channel-fill (Miall, 1978; Walker and Cant, 1984). Trough cross-stratification indicates infilling of a channel by bedload in the form of migrating bedforms (Miall, 1977; Harms et al., 1982; Siegenthaler and Huggenberger, 1993; Kataoka, 2005). Planar cross-bedded sediments are typically interpreted as the deposits of migrating straight-crested dunes, generally formed within the deeper portion of the active channel (Miall, 1985), or by avalanching on the slipfaces of simple bars (Miall, 1996). Such bars may have either been bank-attached (lateral bars) or detached as transverse or medial bars (Todd, 1996). Thus, the deposits of this facies are interpreted as channel-fill in a braided river. Fining-upward sequences resulted from the lateral migration of streams or flow deceleration. Multistoried fining-upward packages with erosional bases suggest frequent channel reactivation with development of bars in fluvial systems. Pebble- to cobble-sized clasts on erosional surfaces were deposited as lag deposit on a channel floor. Clast abrasion in streams was rather inefficient as shown by the subangular to subrounded shapes, which is why it is supposed that all clasts were deposited at a proximal to medial distance from the source area. The fine,

clayey layers on top of this lithofacies point to very low flow energies after relocation of the main channel.

4.2. Rock magnetic properties

The natural remanent magnetization (NRM) of the Tepoztlán Formation samples was previously analyzed by Lenhardt et al. (2010) in order to establish a magnetostratigraphic framework for the formation. NRM intensities range between 0.00059 and 81.16 A/m (average 1.47 A/m). The ferromagnetic minerals within the samples are predominantly titanomagnetites with a relatively low titanium content as was observed during SEM studies (Lenhardt, 2004) and from alternating field (AF) and thermal demagnetization experiments (Lenhardt et al., 2010).

The NRM of the samples mainly consists of one dominating magnetization component, with a small unstable contribution which is removed during the first AF demagnetization steps (0-20 mT). In most cases a characteristic remanence direction was determined with sufficient precision to assign a magnetic polarity (Lenhardt et al., 2010).

Remanence acquisition for lava (depositional temperature above 600°C) and tuff (depositional temperature between 200 and 400°C) was through thermoremanent magnetization (TRM) or partial TRM, and is acquired by a rock during cooling from a temperature above Curie temperature in an external magnetic field (Merrill et al., 1998). Fluvial and mass-flow deposits (deposition at ambient air temperature) are characterised by detrital or depositional remanent magnetization (DRM), acquired by sediments when grains settle in water in the presence of an external magnetic field (Merrill et al., 1998).

Comparison of the data before and after demagnetization showed that the preferred polarity of NRM did not change (Lenhardt et al., 2010), indicating that the NRM is a reliable record of the magnetic field polarity.

4.3. Anisotropy of magnetic susceptibility

The AMS parameters are listed in Table 1. For all analyzed samples the mean bulk susceptibility ranges from 1.18 x 10^{-4} to 1.18 x 10^{-2} [SI] with lava samples yielding the highest values. The anisotropy ratios exhibit P_j values between 1.002 and 1.185 (mean 1.032) and are within the range of usual values for volcanic rocks (e.g., Alva-Valdivia et al., 2005). Except for five samples (TL 5, TL 9, SA 4, SA 26, TE 9) with prolate ellipsoids ($-0.178 \leq T \leq -0.008$) all ellipsoids are oblate ($0.003 \leq T \leq 0.667$; Fig. 3).

The highest mean foliation values within the Tepoztlán Formation can be found in lavas (1.04) followed by tuffaceous breccias (1.03), sandstones (1.02) and tuffs (1.01). In contrast the lineation values of the samples are fairly similar and all four lithologies show mean values of 1.01 (Table 1, Fig. 3b).

Stereographic projections of the lava samples show that axial orientations are either well grouped into clusters (sometimes elongated) or the maximum and intermediate axes form a girdle. If K_1 axes are grouped to clusters they can be either parallel (SAC, Fig. 4) or perpendicular (TE 11, Fig. 4) to the flow plane. The fabrics of the tuffs are similar to those of clastic sediments and were developed during deposition. Clustering of K_3 axes can be observed near the center of the stereographic projection while K_1 and K_2 axes form a girdle close to the horizontal plane (within 10-20°). Stereographic projections of the tuffaceous breccia samples show clustering of the K_1 axes but with relatively high scatter and high angles, while maximum and intermediate axes tend to form girdles. Because of the relatively high scatter the correct flow directions of some of the tuffaceous breccia samples are uncertain. AMS fabrics from most sandstone samples show a good clustering, but clusters of K_1 and K_2 axes are distributed along a great circle in a stereonet plot (Fig. 4).

- place **Table 1** near here -

- place **Figure 3** near here -

- place **Figure 4** near here -

4.4. Field measurements

Within the Tepoztlán Formation, a total of 249 paleocurrent directions were measured from a variety of primary sedimentary structures, i.e. trough cross-stratification, asymmetric ripple marks (from three-dimensional exposures) and the shape of scours (behind blocks and boulders) and channels in sandstones and conglomerates. Paleocurrent directions are shown for 38 units within the three Members of the Tepoztlán Formation (Figs. 5, 6; Table 2).

Within the Malinalco Member, sedimentary structures of fluvial deposits in the Malinalco (MAL) and San Andrés (SAN) sections show flow directions to the SSE and NE, respectively (Figs. 2, 6).

The fluvial deposits of the Malinalco Member show a bimodal distribution with generally two main flow directions of 70° and 135°, a mean transport direction to the ESE (106°) and a standard deviation of 35.5° (Table 2). The variability of the main vectors probably records the shifting back and forth of channel bars in response to alleviation of the gradually subsiding basin floor (Khan and Tewari, 2011).

Within the San Andrés Member, two depositional systems are present: a braided-river system, which dominated the deposition in the Malinalco Member, and a volcanic ring-plain system, introducing volcanic material from its source in the north (Lenhardt et al., 2011). Especially in the western part of the study area (MAL section), the roughly W-E flow direction can still be followed within the fluvial sediments while in the eastern portion (TEP, SOM, TON

sections; Figs. 2, 6) increasingly N-S trending directions can be recorded. The sedimentary structures of the braided-river system show a mean transport direction to the E (85°) with a standard deviation of 48.6°. Sediments of the volcanic ring-plain show a mean direction to the S (186°) with standard deviation of 60.5°.

The Tepozteco Member shows transport direction of braided-river deposits to the E with a mean direction of 116° and a standard deviation of 57.3°. However, an increasingly dominant input of material from the northern volcanic ring-plain can be noted with sedimentary structures showing transport to the south, with a mean direction of 181° and standard deviation of 36.7° (Fig. 5).

Paleocurrent directional data are commonly used to interpret channel sinuosity (Ghosh, 2000; Le Roux, 2001). A low dispersion in paleocurrent values is consistent with a low-sinuosity or braided stream interpretation (Bridge, 1985). A higher dispersion of values can indicate deposition in higher sinuosity or meandering stream settings (Bluck, 1971). Bridge et al. (2000) suggest a relationship between paleocurrent range and channel sinuosity.

Applying two methods, the circular arc and sine-generated curve, the sinuosity (S) can be estimated by using φ, which is half of the maximum paleocurrent range in radians. The equation for sinuosity using the circular arc method is:

$$S = \phi / \sin \phi$$

The equation for calculating sinuosity with the sine-generated curve method is:

$$S = 4.84 / \left(4.83 - \phi^2\right)$$

However, instead of using the maximum paleocurrent range as suggest by Bridge et al. (2000), Le Roux (1992, 1994) recommended the use of the circular standard deviation. This is because the use of the total range of all paleocurrent data may result in overestimation of sinuosity. According to McLaurin and Steel (2007), sinuosity can be better approximated by using standard deviation. Using both methods of Bridge et al. (2000), the sinuosity within the

Malinalco Member was 1.1, the San Andrés Member of 1.2 and the Tepozteco Member of 1.2. The range of sinuosity values is consistent with deposition in an "intermediate sinuosity" setting as described by Miall (1996).

- place **Table 2** near here -

- place **Figure 5** near here -

5. Discussion

5.1. Comparison of the AMS results of the different rock types with the sedimentological paleocurrent indicators

Amongst the Tepoztlán Formation, the best AMS results (including the smallest values for α_{95}) were obtained from lava samples which have the lowest dispersion with average confidence angles of 8° for K_1, 12° for K_2 and 8° for K_3 and the smallest confidence ellipsoids. Lava flow lineations tend to be variable, being either parallel or perpendicular to flow direction. On the other hand, the foliation planes usually show imbrication relative to flow direction. Hargraves et al. (1991) proposed that AMS in lavas (and welded ignimbrites; Wolff et al., 1989) can be issued from an anisotropy of distribution caused by a silicate "template", i.e. a crystallization of titanomagnetite that is controlled by the silicate framework with interstitial magnetite grains crystallizing both along and perpendicular to the lineation of earlier crystallized minerals such as plagioclase (cf., Archanjo et al., 2002). Processes of drag and collisions between adjacent grains within a viscous flow could also result in the creation

of openings and closings normal to extensional direction (Launeau and Cruden, 1998). Thus the occurrence of elongated aggregates of titanomagnetite oriented perpendicular to the plagioclase alignment could generate the perpendicular orientation of the K_1 axis. Bascou et al. (2005) suggested that the lower part of a lava flow is the best region to obtain flow direction from AMS because of parallelism between the crystallographic and magnetic foliation in this part of the flow.

Tuffs and sandstones produce similarly good results with oblate fabrics and foliation planes with imbrication relative to flow direction. Branney and Kokelaar (2002) proposed that ash-flow tuffs are deposited by progressive aggradation. The "sedimentary" characteristics of the tuffs appear to be most marked in the basal layers with closely clustered AMS axes and increasing scatter of the data up-section that can be approximately correlated with increased grain size in the deposits. Tarling and Hrouda (1993) suggest that this might reflect the effects of hydrodynamic and gravitational forces when individual grains are fluidized by a high natural gas content and entrained gases during laminar flow immediately above the depositional interface. Alternatively, it may be because the maximum shear force between the pyroclastic current and its substrate is developed in the early stages of flow, or because deposition in the early stages of the pyroclastic flow is fundamentally different, and slower, than later deposition (LaBerge et al., 2009). Unconfined pyroclastic density currents may initially flow as "sheets" across a relatively planar substrate, but over time the flow will develop channels of higher capacity and velocity (Branney and Kokelaar, 2002). At site TL4, K_1 is perpendicular to flow direction, suggesting magnetic mineral grains became aligned by rolling along the depositional surface. At sites MA3 and SO3, K_1 is approximately parallel to the flow direction, suggesting that grains were sliding along the depositional surface (cf., LaBerge et al., 2009). LaBerge et al. (2009) described an alternation of these interpreted behaviours even within a single flow unit, suggesting evolving conditions within the pyroclastic density current producing grain re-alignment by a variety of mechanisms.

In fluvial deposits the AMS fabrics and eigenvector shapes differ significantly between coarse- and fine-grained deposits (cf., Veloso et al., 2007). Both the corrected anisotropy degree (P_j) and the magnetic foliation (F) increase with a decrease in grain size (Liu et al., 2001). In general, AMS fabrics from sandstone sites are typical of those formed by medium to low velocity flows, whereas fabrics from conglomerates and mudstones are typical of high and low velocity flows, respectively (e.g., Liu et al., 2001).

Sedimentological paleocurrent indicators (trough cross-stratification, asymmetric ripples, the shape of scours and channels) in sandstones and conglomerates are similar to AMS measurements in these sediments and can thus be used to verify AMS results. Differences between data from closely related fluvial strata can be explained by channel shifting or the meeting of river systems with divergent flow directions. Transverse bars may also migrate perpendicular to the general river flow (Miall, 1985). In the tuffs the only useable sedimentary structures were sag structures beneath ballistic blocks and bombs but these are not diagnostic of flow direction. For these massive and poorly sorted volcaniclastic rocks, AMS measurements are often the only way of finding reliable transport directions.

- place **Figure 6** near here -

5.2. Source vent locations and river provenance

The magnetic fabrics of the Tepoztlán Formation samples can also be used to indicate sediment source direction. At most sites, tilting direction of the K_3 axis and the azimuth of magnetic lineation are consistent with sediment source direction as deduced from sedimentary structures. The accuracy of AMS in pyroclastic rocks could be partly supported by their closeness to their suspected source areas and through analysis of lateral facies distributions (Lenhardt et al., 2011).

Within the Malinalco Member, magnetic fabrics of sandstones show river flow direction towards the E/SE, which is consistent with measurements of sedimentary structures (Fig. 6). Lenhardt et al. (2011) describe the depositional setting as a low-sinuosity channel system with high-sediment-laden debris flows and hyperconcentrated flows, originating from several volcanoes after heavy rains. The W-E trending axial braided-river system can be explained by the La Pera fault system, which has existed since pre-Miocene times (Johnson and Harrison, 1990; Garduno et al., 1993).

The AMS measurements on pyroclastic rocks in Malinalco suggest a volcanic center SE of that town. Vent breccias and radial dikes are consistent with this source region. AMS fabrics of a lava flow show a southward flow direction, thus a source to the north.

Paleocurrent data from the San Andrés sections (SAN1+2) suggest that a volcanic center must have existed north of Tepoztlán. The San Andrés Member shows a similar pattern of AMS fabrics to the Malinalco Member, suggesting volcanic sources to the SE and N. AMS measurements on tuffs in the San Andrés member suggest a point source in the present-day Sierra Chichinautzin, where the proto-edifice may be buried below modern lava flows. In the Malinalco Member, AMS measurements on thin tuffs point to a volcanic source to the NE, suggesting a coalescing of the ring plains of two different volcanoes near present-day Tlajotlán. The most probable volcanic source NE of Malinalco is a precursor of the present-day Zempoala Complex (Fries, 1960), as suggested by De Cserna and Fries (1981). The Zempoala volcanic region is furthermore supposed the likely source of massive lava flows near Ahuatenco (K/Ar ages of 22.4±0.5 Ma, 21.9± 0.5 Ma; Lenhardt et al., 2010). Here, the lava (30 m thick) flowed southward into a pre-existing depression, reaching a maximum thickness of 400 m. AMS measurements within the Tepozteco Member indicate point sources of volcanic material, north of Tepoztlán and north of the village San Agustín (Fig. 6). Paleocurrent data indicate that basin sedimentation underwent a significant change from a predominantly W-E trending fluvial to a N-S trending mass-flow depositional system. The

influence of the ring-plain increased and dominated the axial fluvial system during this period (Lenhardt et al., 2011). This can be seen within the TEP section, which is interpreted as the active part of the volcanic ring-plain, developing at the southern edge of a prominent volcanic edifice (Lenhardt, 2009). Deposition near San Agustín was influenced by a volcanic center relatively close to location SAG itself but now covered by lavas of the Chichinautzin Formation. Volcanic products are interpreted to come from a lateral parasitic vent at the southeastern flank of the Chichinautzin proto-edifice, which had reached a critical height at this time in terms of slope stability and magma ascent.

6. Conclusion

Within the study area it was possible to document directional results from AMS data as well as sedimentary structures which were used to calibrate AMS data and to prove their reliability. The results of this study show that the most reliable AMS measurements are obtained from lava samples, followed by tuffs and sandstones; the least reliable from tuffaceous breccias deposited by mass flows. Based on comparisons between paleocurrent directions from primary sedimentary structures and AMS data, AMS analysis can be used to determine paleocurrent directions for the Tepoztlán Formation. Differences between data from closely related fluvial strata can be due to channel shifting or convergence of different river systems. The volcanic edifices and their aprons, which acted as sediment sources are located north of Tepoztlán in the Sierra Chichinautzin. Direct evidence for a volcanic centre could only be obtained for the Malinalco Member. In the Sierra Chichinautzin the presumable centres are buried by younger volcanic deposits. Sedimentary structures and paleocurrent directions of sandstones show that a W-E trending braided river system dominated the study area between 22.8 and 22.2 Ma before it was covered by aggradational ring-plains of at least three stratovolcanoes.

Acknowledgements

This research work is modified from a part of the Doctoral thesis of the first author (Lenhardt, 2009), carried out at the Technische Universität Darmstadt, Germany, as part of a cooperative project with the Universidad Nacional Autónoma de México (UNAM), Mexico. The study was funded by the Deutsche Forschungsgemeinschaft (DFG), project HI 643/5-1. H. Böhnel acknowledges support by Conacyt (grant 46213). We thank José Luis Rodríguez Vargas, Iván Barajas Gea and Gildardo González Naranjo for assisting in the laboratory measurements at the Centro de Geociencias, Querétaro. Ignacio Torres-Alvarado (Centro de Investigación en Energía, UNAM) is thanked for logistic support. Patrick G. Eriksson (University of Pretoria) is especially thanked for his very helpful comments on an early version of the manuscript. Editors Gert Jan Weltje, Jasper Knight, and two anonymous reviewers are thanked for their criticism and helpful comments.

References

Abdelayem, A.L., Yamazaki, T., Ikehara, K., 1999. Magnetic susceptibility anisotropy and remanence of some deep-sea sediments of Tokai Basin. In: Yuosa, M. (Ed.), Marine Geological Investigations of the Tokai Offshore Area, Geological Survey of Japan, Japan, pp. 127-146.

Allen, J.R.L., 1984. Sedimentary structures – Their character and physical basis. Elsevier, Amsterdam.

Alva-Valdivia, L.M., Rosas-Elguera, J., Bravo-Medina, T., Urrutia-Fucugauchi, J., Henry, B., Caballero, C., Rivas-Sanchez, M.L., Goguitchaichvili, A., López-Loera, H., 2005. Paleomagnetic and magnetic fabric studies of the San Gaspar ignimbrite, western Mexico -

constraints on emplacement mode and source vents. Journal of Volcanology and Geothermal Research 147, 68-80.

Arbaret, L., Diot, H., Bouchez, J.L., 1996. Shape fabric of particles in low concentration suspensions : 2D analogue experiments and application to tiling in magma. Journal of Structural Geology 18, 941-950.

Archanjo, J.A., Araújo, M.G.S., Launeau, P., 2002. Fabric of the Rio Ceará-Mirim mafic dyke swarm (Northeastern Brazil), determined by anisotropy of magnetic susceptibility and image analysis. Journal of Geophysical Research 107, 10,1029-11,1041.

Baer, E.M., Fisher, R.V., Fuller, M., Valentine, G., 1997. Turbulent transport and deposition of the Ito pyroclastic flow: determinations using anisotropy of magnetic susceptibility. Journal of Geophysical Research 102, 22,565- 22,586.

Baldsley, J.R., Buddington, A.F., 1960. Magnetic susceptibility anisotropy and frabric of some Adirondack granites and orthogneisses. American Journal of Science 258, 6-20.

Bascou, J., Camps, P., Dautria, J.M., 2005. Magnetic versus crystallographic fabrics in a basalt lava flow. Journal of Volcanology and Geothermal Research 145, 119-135.

Bluck, B.J., 1971. Sedimentation in the meandering River Endrick. Scottish Journal of Geology 7, 93-138.

Bonnichsen, B., Kauffmann, D.F., 1987. Physical features of rhyolite lava flows in the Snake River Plain volcanic province, south-western Idaho. In: Fink, J.H. (Ed.), The emplacement of silicic domes and lava flows. Geological Society of America Special Paper 212, 119-145.

Branney, M.J., Kokelaar, B.P., 2002. Pyroclastic density currents and the sedimentation of ignimbrites. Geological Society London Memoir 27, London, 143 pp.

Bridge, J.S., 1985. Paleochannel patterns inferred from alluvial deposits: a critical evaluation. Journal of Sedimentary Petrology 55, 579-589.

Bridge, J.S., Jalfin, G.A., Georgieff, S.M., 2000. Geometry, lithofacies and spatial distribution of Cretaceous f luvial sandstone bodies, San Jorge Basin, Argentina: outcrop analog for the hydrocarbon-bearing Chubut Group. Journal of Sedimentary Research 70, 341-359.

Cagnoli, B., Tarling, D.H., 1997. The reliability of anisotropy of magnetic susceptibility (AMS) data as flow direction indicators in friable base surge and ignimbrite deposits: Italian examples. Journal of Volcanology and Geothermal Research 75, 309-320.

Cañón-Tapia, E., Castro, J., 2004. AMS measurements on obsidian from the Inyo Domes, CA: a comparison of magnetic and mineral preferred orientation fabrics. Journal of Volcanology and Geothermal Research 134, 169-182.

Cañón-Tapia, E., Walker, G.P.L., 1998. Mecanismo de emplazamiento de las mesetas basálticas gigantes continentales estudiado a través de mediciones de anisotropía de susceptibilidad magnética. Geos 18, 2-10.

Cañón-Tapia, E., Walker, G.P.L., Herrero-Bervera, E., 1996. The internal structure of lava flows – insights from AMS measurements: I. Near-vent a'a. Journal of Volcanology and Geothermal Research 70, 21-36.

Cañón-Tapia, E., Walker, G.P.L., Herrero-Bervera, E., 1997. The internal structure of lava flows – insights from AMS measurements: II. Hawaiian pahoehoe, toothpaste lava and a'a. Journal of Volcanology and Geothermal Research 76, 19-46.

Capaccioni, B., Sarocchi, D., 1996. Computer-assisted image analysis on clast shape fabric from the Orvieto-Bagnoregio ignimbrite (Vulsini District, central Italy): implications on the emplacement mechanisms. Journal of Volcanology and Geothermal Research 70, 75-90.

Cas, R.A.F., Wright, J.V., 1987. Volcanic successions – modern an ancient. Allen & Unwin, London, 528 pp.

Cashman, K.V., Kauahikaua, J.P., 1997. Reevaluation of vesicle distributions in basaltic lava flows. Geology 25, 419-422.

Coussot, P., Meunier, M., 1996. Recognition, classification and mechanical description of debris flows. Earth-Science Reviews 40, 209-227.

Cronin, S.J., Neall, V.E., 1997. A late Quaternary stratigraphic framework for the northeastern Ruapehu and eastern Tongariro ring plains, New Zealand. New Zealand Journal of Geology and Geophysics 40, 185-197.

De Cserna, Z., Fries, C., 1981. Hoja Taxco 14 Q-h (7), con resumen de la geología de la hoja Taxco, estados de Guerrero, México y Morelos: Universidad Autónoma de México, Instituto de Geología, Carta Geológica de México, Serie 1:100 000, map with text, 47 pp.

Dragoni, M., Lanza, R., Tallarico, A., 1997. Magnetic anisotropy produced by magma flow: theoretical model and experimental data from Ferrar dolerite sills (Antarctica). Geophysical Journal International 128, 230-240.

Ellwood, B.B., 1982. Estimates of flow direction for calc-alkaline welded tuffs and paleomagnetic data reliability from anisotropy of magnetic susceptibility measurements: central San Juan Mountains, southwest Colorado. Earth and Planetary Science Letters 59, 303-314.

Ellwood, B.B., Ledbetter, M.T., 1977. Antarctic bottom water fluctuations in the Vema Channel: effects of velocity changes on particle alignment and size. Earth and Planetary Science Letters 35, 189-198.

Ellwood, B.B., Ledbetter, M.T., 1979. Paleocurrent indicators in deep sea sediment. Science 203, 1335-1337.

Ellwood, B.B., Hrouda, F., Wagner, J., 1988. Symposia on magnetic fabrics: introductory comments. Physics of the Earth and Planetary Interiors 51, 249-252.

Elston,W.E., Smith, E.I., 1970. Determination of flow direction of rhyolitic ash-flow tuffs from fluidal textures. Geological Society of America Bulletin 81, 3393-3406.

Fisher, R.V., Orsi, G., Ort, M.H., Heiken, G., 1993. Mobility of a large-volume pyroclastic Flow – emplacement of the Campanian Ignimbrite, Italy. Journal of Volcanology and Geothermal Research 56, 205-220.

Fries, C., 1960. Geología del Estado de Morelos y de partes adyacentes de México y Guerrero, región central meridional de México. Boletín del Instituto Geología, UNAM, 60, 1-236.

Froggatt, P.C., Wilson, C.J.N., Walker, G.P.L., 1981. Orientation of logs in the Taupo ignimbrite as an indicator of flow direction and vent position. Geology 9, 109-111.

García-Palomo, A., 1998. Evolucion estructural en las inmediaciones del Volcan Nevado de Toluca, Edo. De Mexico. M.Sc. thesis, Universidad Autónoma de México, Instituto de Geología, Mexico, 146 pp.

García-Palomo, A., Macías, J.L., Garduno, V.H., 2000. Miocene to recent structural evolution of the Nevado de Toluca volcano region, Central Mexico. Tectonophysics 318, 281-302.

Garduno, V.H., Spinnler, J., Ceragioli, E., 1993. Geological and structural study of the Chapala Rift, state of Jalisco, Mexico. Geofísica Internacional 32, 487-499.

Geoffroy, L., Callot, J.P., Aubourg, C., Moreira, M., 2002. Magnetic and plagioclase linear fabric discrepancy in dykes: a new way to define the flow vector using magnetic foliation. Terra Nova 14, 183-190.

Ghosh, P., 2000. Estimation of channel sinuosity from paleocurrent data: a method using fractal geometry. Journal of Sedimentary Research 70, 449-455.

Halvorsen, E., 1974. The magnetic fabric of some dolerite intrusions, northeast Spitsbergen, implications fort he emplacement. Earth and Planetary Science Letters 21, 127-133.

Hampton, M.A., 1975. Competence of fine-grained debris flows. Journal of Sedimentary Petrology 45, 834-844.

Hargraves, R.B., Johnson, D., Chan, C.Y., 1991. Distribution anisotropy : the cause of AMS igneous rocks? Geophysical Research Letters 18, 2193-2196.

Harms, J.C., Southard, J.B., Spearing, D.R., Walker, R.G., 1982. Depositional environments as interpreted from primary sedimentary structures and stratification sequences. Lecture Notes, Society of Economic Paleontologists and Mineralogists, Short Course 2, Dallas, 161 pp.

Herrero-Bervera, E., Cañón-Tapia, E., Walker, G.P.L., Tanaka, H., 2002. Magnetic fabric study and inferred flow directions of lavas of the Old Pali Road, O'ahu, Hawaii. Journal of Volcanology and Geothermal Research 118, 161-171.

Hillhouse, J.W., Wells, R.E., 1991. Magnetic fabric, flow directions, and source area of the lower Miocene Peach Springs Tuff in Arizona, California, and Nevada. Journal of Geophysical Research 96, 12,443-12,460.

Hrouda, F., 1982. Magnetic anisotropy of rocks and its application in geology and geophysics. Surveys in Geophysics 5, 37-82.

Iezzi, G., Ventura, G., 2002. Crystal fabric evolution in lava flows: results from numerical simulations. Earth and Planetary Science Letters 200, 33-46.

Incoronato, A., Addison, F.T., Tarling, D.H., Nardi, G., Pescatore, T., 1983. Magnetic fabric investigations of pyroclastic deposits from Phlegrean Fields, southern Italy. Nature 306, 461-463.

Ising, G., 1942. On the magnetic properties of varved clay. Arkiv för matematik, astronomi och fysik 29, 1-37.

Jelinek, V., 1978. Statistical processing of magnetic susceptibility measured on groups of specimens. Journal of Geomagnetism and Geoelectricity 22, 50-62.

Jelinek, V., 1981. Characterization of the magnetic fabric of rocks. Tectonophysics 79, 63-67.

Johnson, C., Harrison, C., 1990. Neotectonics in central Mexico. Physics of the Earth and Planetary Interiors 64, 187-210.

Johnson, A.M., Rodine, J.R., 1984. Debris Flow. In: Brunsden, D., Prior, D.B. (Eds.), Slope Instability. Wiley, Chichester, pp. 257-361.

Kataoka, K., 2005. Distal fluvio-lacustrine volcaniclastic resedimentation in response to an explosive silicic eruption: The Pliocene Mushono tephra bed, Central Japan. Geological Society of America Bulletin 117, 3-17.

Khan, Z.A., Tewari, R.C., 2011. Paleochannel and paleohydrology of a Middle Siwalik (Pliocene) fluvial system, northern India. Journal of Earth System Science 120, 531-543.

Knight, M.D., Walker, G.P.L., Ellwood, B.B., Diehl, J.F., 1986. Stratigraphy, paleomagnetism and magnetic fabric of the Toba Tuffs: constraints on the sources and eruptive styles. Journal of Volcanology and Geothermal Research 56, 205-220.

Kolofikova, O., 1976. Geological interpretation of measurement of magnetic properties of basalts on example of the Chrobsky les lava flow of the Veljy Roudny volcano (Nizky Jesenik Mts.) Casopis pro Mineralogii a Geologii 21, 387-396 (in Czech).

LaBerge, R.D., Porreca, M., Mattei, M., Giordano, G., Cas, R.A.F., 2009. Meandering flow of a pyroclastic density current documented by the anisotropy of magnetic susceptibility (AMS) in the quartz latite ignimbrite of the Pleistocene Monte Cimino volcanic centre (central Italy). Tectonophysics 466, 64-78.

Launeau, P., Cruden, A.R., 1998. Magmatic fabric acquisition mechanisms in a syenite: results of a combined anisotropy of magnetic susceptibility and image analysis study. Journal of Geophysical Research 103, 5067-5089.

Le Pennec, J.-L., Chen, Y., Diot, H., Froger, J.-L., Gourgaud, A., 1998. Interpretation of anisotropy of magnetic susceptibility fabric of ignimbrites in terms of kinematic and

sedimentological mechanisms: an Anatolian case-study. Earth and Planetary Science Letters 157, 105-127.

Le Roux, J.P., 1992. Determining the channel sinuosity of ancient fluvial systems from paleocurrent data. Journal of Sedimentary Petrology 62, 283-291.

Le Roux, J.P., 1994. The angular deviation of paleocurrent directions as applied to the calculation of channel sinuosities. Journal of Sedimentary Research 64, 86-87.

Le Roux, J.P., 2001. Estimation of channel sinuosity from paleocurrent data: a method using fractal geometry – discussion. Journal of Sedimentary Research 71, 1029-1030.

Lee, I., Ogawa, Y., 1998. Bottom-current deposits in the Miocene-Pliocene Misaki Formation, Izu forearc area, Japan. The Island Arc 7, 315-329.

Lenhardt, N., 2004. Sedimentologische und palynologische Untersuchungen im Bereich der Typlokalität der volkanoklastischen Formacíon Tepoztlán (Morelos, Mexico). M.Sc. Thesis, Technical University of Darmstadt, Germany.

Lenhardt, N., 2009. Volcaniclastic successions of the southern edge of the Transmexican Volcanic Belt: evidence for the Miocene plate reorganisation in Central America (Morelos, Mexico). Ph.D. Thesis, Technical University of Darmstadt, Germany. 141 pp. URL: http://tuprints.ulb.tu-darmstadt.de/1405/

Lenhardt, N., Böhnel, H., Wemmer, K., Torres-Alvarado, I.S., Hornung, J., Hinderer, M., 2010. Petrology, magnetostratigraphy and geochronology of the Miocene

volcaniclastic Tepoztlán Formation: implications for the initiation of the Transmexican Volcanic Belt (Central Mexico). Bulletin of Volcanology 72, 817-832.

Lenhardt, N., Hornung, J., Hinderer, M., Böhnel, H., Torres-Alvarado, I.S., Trauth, N., 2011. Build-up and depositional dynamics of an arc front volcaniclastic complex: The Miocene Tepoztlán Formation (Transmexican Volcanic Belt, Central Mexico). Sedimentology 58, 785-823.

Liu, B., Saito, Y., Yamazaki, T., Abdelayem, A., Oda, H., Hori, K., Zhao, Q., 2001. Paleocurrent analysis for the Late Pleistocene-Holocene incised-valley fill of the Yangtze delta, China by using anisotropy of magnetic susceptibility data. Marine Geology 176, 175-189.

Liu, B., Saito, Y., Yamazaki, T., Abdelayem, A., Oda, H., Hori, K., Zhao, Q., 2005. Anisotropy of Magnetic Susceptibility (AMS) characteristics of tide-influenced sediments in the Late Pleistocene-Holocene Changjiang incised-valley fill, China. Journal of Coastal Research 21, 1031-1041.

MacDonald, G.A., 1972. Volcanoes. Prentice-Hall, Engelwood Cliffs, NJ, 510 pp.

MacDonald, W.D., Palmer, H.C., 1990. Flow directions in ash-flow tuffs: a comparison of geological and magnetic susceptibility measurements, Tshirege member (upper Bandelier Tuff), Valles caldera, New Mexico, USA. Bulletin of Volcanology 53, 45-59.

MacDonald, W.D., Palmer, H.C., Hayatsu, A., 1992. Egan Range Volcanic Complex, Nevada: geochronology, paleomagnetism and magnetic fabric. Physics of the Earth and Planetary Interiors 74, 109-126.

MacDonald, W.D., Palmer, H.C., Hayatsu, A.,1998. Structural rotation and volcanic source implications of magnetic data from Eocene volcanic rocks, SW Idaho. Earth and Planetary Science Letters 156, 225-237.

Manga, M., 1998. Orientation distribution of microlites. Journal of Volcanology and Geothermal Research 86, 107- 115.

Manville, V., Németh, K., Kano, K., 2009. Source to sink: A review of three decades of progress in the understanding of volcaniclastic processes, deposits, and hazards. Sedimentary Geology 220, 136-161.

Márquez, A., Verma, S., Anguita, F., Oyarzun, R., Brandle, J., 1999. Tectonics and volcanism of Sierra Chichinautzin: Extension at the front of the central transmexican volcanic belt. Journal of Volcanology and Geothermal Research 93, 125-150.

McLaurin, B.T., Steel, R.J., 2007. Architecture and origin of an amalgamated fluvial sheet sand, lower Castlegate Formation, Book Cliffs, Utah. Sedimentary Geology 197, 291-311.

McPhie, J., Doyle, M., Allen, R., 1993. Volcanic textures – a guide to the interpretation of textures in volcanic rocks. Centre for Ore Deposit and Exploration Studies, University of Tasmania, pp. 1-198.

Merrill, R.T., McElhinny, M.W., McFadden, P.L., 1998. The magnetic field of the earth – Paleomagnetism, the core, and the deep mantle. International Geophysics series 63, Academic Press, New York, pp. 1-531.

Miall, A.D., 1977. A review of the braided river depositional environment. Earth-Science Reviews 13, 1-62.

Miall, A.D., 1978. Lithofacies types and vertical profile models in braided rivers: a summary. Canadian Society of Petroleum Geologists Memoir 5, 597-604.

Miall, A.D., 1985. Architectural-element analysis: a new method of facies analysis applied to fluvial deposits. Earth-Science Reviews 22, 261-308.

Miall, A.D., 1996. The Geology of fluvial Deposits. Springer-Verlag, Berlin. 582 pp.

Moreira, M., Geoffroy, L., Pozzi, J.P., 1999. Écoulement magmatique dans les dykes du point chaud des Açores : étude préliminaire par anisotropie de susceptibilité magnétique (AMS) dans l'île de San Jorge. Comptes Rendus de l'Académie des Sciences, Paris 329, 15-22.

Mueller, W., 1991. Volcanism and related slope to shallow marine volcaniclastic sedimentation: an Archean example Chibougamau, Quebec, Canada. Precambrian Research 49, 1-22.

Nagata, T., 1961. Rock magnetism, 2nd ed. Maruzen, Tokyo.

Ort, M.H., 1993. Eruptive processes and caldera formation in a nested downsag-collapse caldera: Cerro Panizos, central Andes Mountains. Journal of Volcanology and Geothermal Research 56, 221-252.

Ort, M.H., Rosi, M., Anderson, C.D., 1999. Correlation of deposits and vent locations of the proximal Campanian Ignimbrite deposits, Campi Flegrei, Itali, based on natural remanent magnetization and anisotropy of magnetic susceptibility characteristics. Journal of Volcanology and Geothermal Research 91, 167-178.

Ort, M.H., Orsi, G., Pappalardo, L., Fisher, R.V., 2003. Anisotropy of magnetic susceptibility studies of depositional processes in the Campanian Ignimbrite, Italy. Bulletin of Volcanology 65, 55-72.

Orton, G.J., 1996. Volcanic environments. In: Reading, H.G. (Ed.), Sedimentary Environments: Processes, Facies and Stratigraphy. Blackwell Science, Oxford, pp. 485-567.

Palmer, B.A., 1991. Holocene lahar deposits in the Whakapapa catchment, northwestern ring plain, Ruapehu volcano (North Island, New Zealand). New Zealand Journal of Geology and Geophysics 34, 177-190.

Palmer, H.C., MacDonald,W.D., 1999. Anisotropy of magnetic susceptibility in relation to source vents of ignimbrites: empirical observations. Tectonophysics 307, 207-218.

Palmer, B.A., Neall, V.E., 1991. Contrasting lithofacies architecture in ring-plain deposits related to edifice construction and destruction, the Quaternary Stratford and Opunake Formations, Egmont Volcano, New Zealand. Sedimentary Geology 74, 71-88.

Palmer, B.A., Purves, A.M., Donoghue, S.L., 1993. Controls on accumulation of a volcaniclastic fan, Ruapehu composite volcano, New Zealand. Bulletin of Volcanology 55, 176-189.

Park, J.K., Tanczyk, E.I., Desbarats, A., 1988. Magnetic fabric and its significance in the 1400 Ma mealy diabase dykes of Labrador, Canada. Journal of Geophysical Research 93, 13689-13704.

Park, C.-K., Doh, S.-J., Suk, D.-W., Kim, K.-H., 2000. Sedimentary fabric on deep-sea sediments from KODOS area in the eastern Pacific. Marine Geology 171, 115-126.

Pierson, T.C., Daag, A.S., Reyes, P.J.D., Regalado, M.T.M., Solidum, R.U., Tubianosa, B.S., 1996. Flow and deposition of post-eruption hot lahars on the east side of Mount Pinatubo, July-October 1991. In: Newhall, C.G., Punongbayan, R.S. (Eds.), Fire and Mud, Eruptions and Lahars of Mount Pinatubo, Philippines. Philippines Institute of Volcanology and Seismology, Univ. Washington Press, pp. 921-950.

Piper, J.D.A., Elliot, M.T., Kneller, B.C., 1996. Anisotropy of magnetic susceptibility in a Paleozoic flysch basin: the Windermere Supergroup, northern England. Sedimentary Geology 106, 235-258.

Potter, D.K., Stephenson, A., 1988. Single particles in rocks and magnetic fabric analysis. Geophysical Research Letters 15, 1097-1100.

Reading, H.G., 1996. Sedimentary environments: Processes, facies and stratigraphy, 3rd ed. Blackwell, Osney Mead, Oxford.

Rees, A.I., 1965. The use of anisotropy of magnetic susceptibility in the estimation of sedimentary fabric. Sedimentology 4, 257-271.

Rees, A., Woodall, W., 1975. The magnetic fabric of some laboratory-deposited sediments. Earth and Planetary Science Letters 25, 121-130.

Reineck, H.-E., Singh, I.B., 1980. Depositional sedimentary environments, 2nd revised and updated ed. Springer, Berlin.

Rochette, P., Jackson, M., Aubourg, C., 1992. Rock magnetism and the interpretation of anisotropy of magnetic susceptibility. Reviews of Geophysics 30, 209-226.

Rochette, P., Aubourg, C., Perrin, M., 1999. Is this magnetic fabric normal? A review and case studies in volcanic formations. Tectonophysics 307, 219-234.

Ross, C.S., Smith, R.L., 1961. Ash-flow tuffs. Their origin, Geological Relations and Identification. U.S. Geological Survey Professional Paper 366, 81 pp.

Seaman, S.J., McIntosh, W.C., Geissman, J.W., Williams, M.L., Elston, W.E., 1991. Magnetic fabrics of the Bloodgood Canyon and Shelley Peak Tuffs, southwestern New Mexico: implications for emplacement and alteration processes. Bulletin of Volcanology 53, 460-476.

Siebe, C., Macías, J.L., 2004. Volcanic hazards in the Mexico City metropolitan area from eruptions at Popocatépetl, Nevado de Toluca, and Jocotitlán stratovolcanoes and monogenetic scoria cones in the Sierra Chichinautzin Volcanic Field. Penrose Field Guide: Penrose Field Guide 1, 77 pp.

Siebe, C., Rodríguez-Lara, V., Schaaf, P., Abrams, M., 2004. Geochemistry, Sr-Nd isotope composition, and tectonic setting of Holocene Pelado, Guespalapa and Chichinautzin scoria cones, south of Mexico City. Journal of Volcanology and Geothermal Research 130, 197-226.

Siegenthaler, C., Huggenberger, P., 1993. Pleistocene Rhine gravel: deposits of a braided river system with dominant pool preservation. In: Best, J.L., Bristow, C.S. (Eds.), Braided Rivers. Geological Society Special Publication 75, 147-162.

Smith, S.A., 1990. The sedimentology and accretionary style of an ancient gravel-bed stream: the Budleigh Salterton Pebble Beds (Lower Triassic), southwest England. Sedimentary Geology 67, 199-219.

Smith, G.A., Lowe, D.R., 1991. Lahars: volcano-hydrologic events and deposition in the debris flow – hyperconcentrated flow continuum In: Fisher, R.V., Smith, G.A. (Eds.), Sedimentation in Volcanic Settings. Society of Economic Paleontologists and Mineralogists, Special Publication 45, 59-70.

Smith, E.I., Rhodes, R.C., 1972. Flow direction determination of lava flows. Geological Society of America Bulletin 83, 1869-1873.

Sparks, R.S.J., 1976. Grain size variations in ignimbrites and implications for the transport of pyroclastic flows. Sedimentology 23, 147-188.

Stacey, F.D., Joplin, G., Lindsay, J., 1960. Magnetic anisotropy and fabric of some foliated rocks from SE Australia. Pure and Applied Geophysics 47, 30-40.

Steel, R.J., Thompson, D.B., 1983. Structures and textures in Triassic braided stream conglomerates ('Bunter' Pebble Beds) in the Sherwood Sandstone Group, North Staffordshire, England. Sedimentology 30, 341-367.

Stephenson, A., 1994. Distribution anisotropy: two simple models for magnetic lineation and folation. Phys. Physics of the Earth and Planetary Interiors 82, 49-53.

Tarling, D.H., Hrouda, F., 1993. The Magnetic Anisotropy of Rocks. Chapman and Hall, London, pp. 1-217.

Tarling, D.H., Shi, H., 1995. Magnetic anisotropy of borehole core samples. In: Turner, P., Turner, A. (Eds.), Palaeomagnetic Applications in Hydrocarbon Exploration and Production. Geological Society London Special Publication 98, 273-280.

Todd, S.P., 1996. Process deduction from fluvial sedimentary structures. In: Carling, P.A., Dawson, M.R. (Eds.), Advances in Fluvial Dynamics and Stratigraphy. Wiley, Chichester, pp. 299-350.

Veloso, E.E., Anma, R., Ota, T., Komiya, T., Kagashima, S., Yamazaki, T., 2007. Paleocurrent patterns of the sedimentary sequence of the Taitao ophiolite constrained by

anisotropy of magnetic susceptibility and paleomagnetic analyses. Sedimentary Geology 201, 446-460.

Walker, G.P.L., 1989. Spongy pahoehoe in Hawaii: a study of vesicle-distribution patterns in basalt and their significance. Bulletin of Volcanology 51, 199-209.

Walker, R.G., Cant, D.J., 1984. Sandy fluvial systems. In: Walker, R.G., (Ed.), Facies Models, 2nd edition, Geoscience Canada Reprint Series 1, pp. 71-89.

Waters, A.C., 1960. Determining direction of flow in basalts. American Journal of Science 258, 350-360.

Williams, H., McBirney, A.R., 1979. Volcanology. Freeman and Cooper, San Francisco, Calif., 391 pp.

Wilson, C.J.N., Walker, G.P.L., 1982. Ignimbrite depositional facies: the anatomy of a pyroclastic flow. Journal of the Geological Society 139, 581-592.

Wing-Fatt, L., Stacey, F.D., 1966. Magnetic anisotropy of laboratory materials in which magma flow is simulated. Pure and Applied Geophysics 64, 78-80.

Wolff, J.A., Ellwood, B.B., Sachs, S.D., 1989. Anisotropy ofmagnetic susceptibility inwelded tuffs: application to a welded-tuff dyke in the Tertiary Trans-Pecos Texas volcanic province, USA. Bulletin of Volcanology 51, 299-310.

Zanella, E., De Astis, G., Dellino, P., Lanza, R., La Volpe, L., 1999. Magnetic fabric and remanent magnetization of pyroclastic surge deposits from Vulcano (Aeolian Islands, Italy). Journal of Volcanology and Geothermal Research 93, 217-233.

Zhu, R., Shi, C., Liu, Q., 2003. Anisotropy of magnetic susceptibility of Hannuaoba basalt, northern China: constrain on the vent position of the lava sequences. Geophysical Research Letters 30, 38-1-38-4.

Figures:

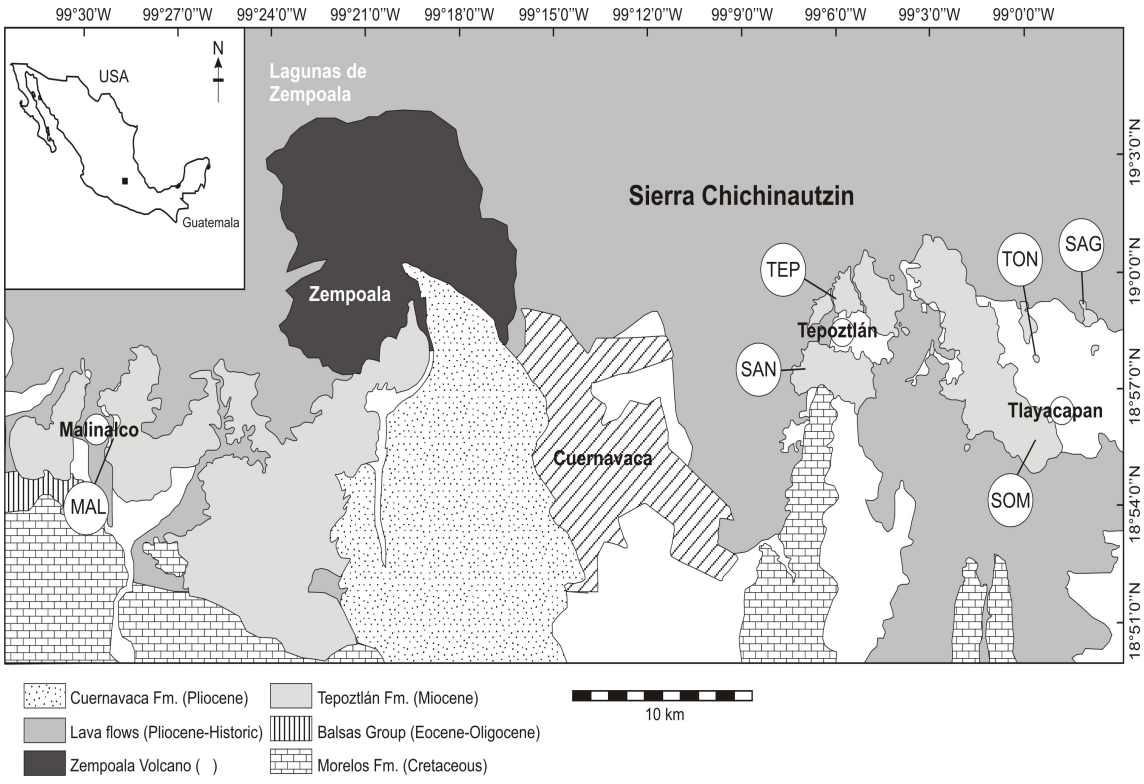

Figure 1. Geological map of the study area with locations of the sampled stratigraphic sections: MAL – Malinalco; TEP – Tepozteco; SAN – San Andrés; SOM – Cerro Sombrerito; TON – Cerro Tonantzin; TLA – San Agustín. The inset shows the location of the study area within Mexico.

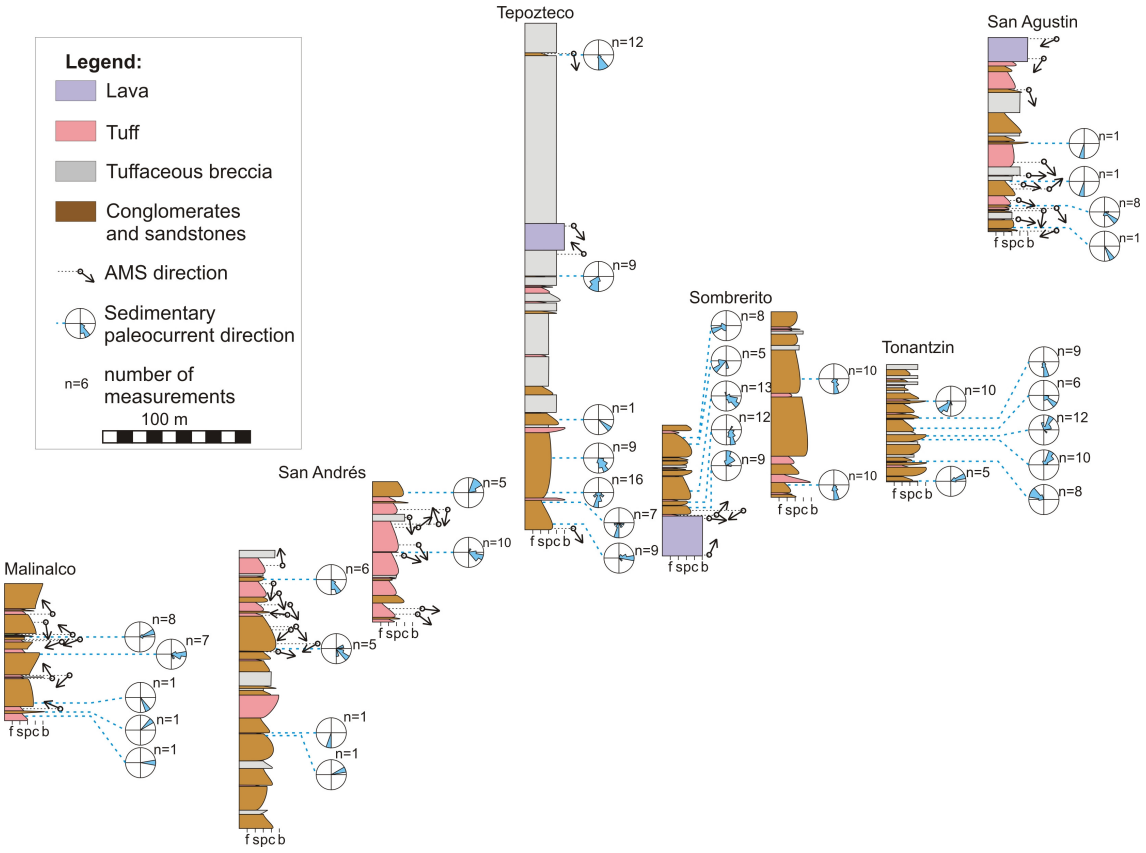

Figure 2. Stratigraphy of the Tepoztlán Formation conducted over 56 km along strike, showing correlations between outcrops and sampling sites including measured paleocurrent indicators. The locations of the sections are indicated in Fig. 1. f, fines; s, sand; p, pebbles; c, cobbles; b, boulders.

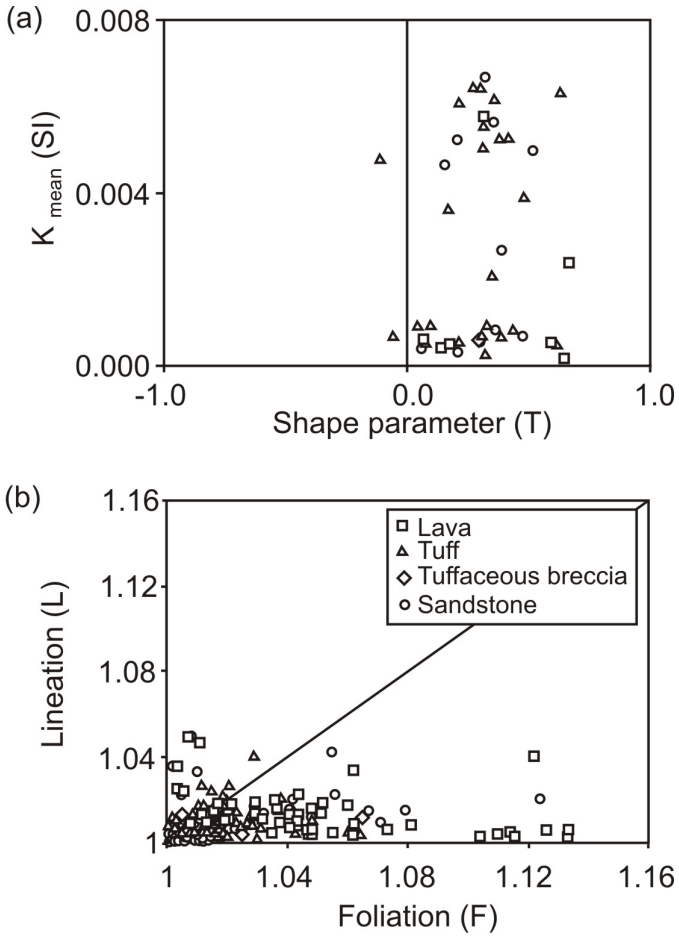

Figure 3. AMS parameters. a) Shape Parameter (T) vs. the Degree of Anisotropy (P) (Jelinek, 1981; Hrouda, 1982). b) Lineation (L) (Baldsely and Buddington, 1960) vs. Foliation (F) (Stacey et al., 1960).

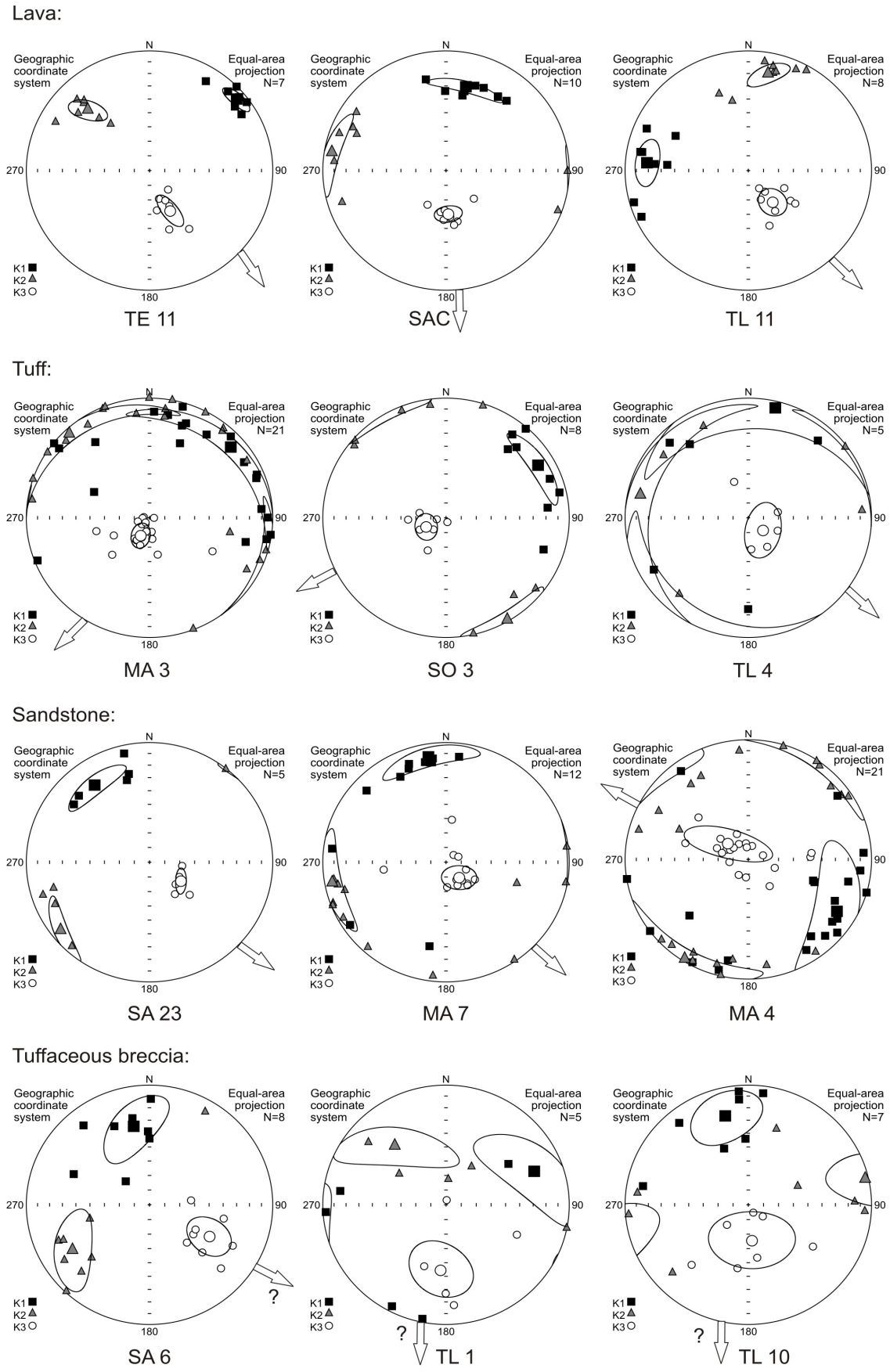

Figure 4. Examples of magnetic fabrics associated with Tepoztlán Formation samples of lava, tuff, tuffaceous breccia and sandstone. Minimum susceptibility axes (circles) are tilted in the flow direction (white arrows show the direction of flow) while the maximum susceptibility axes (squares) form a girdle or are aligned either parallel or perpendicular to the direction of flow.

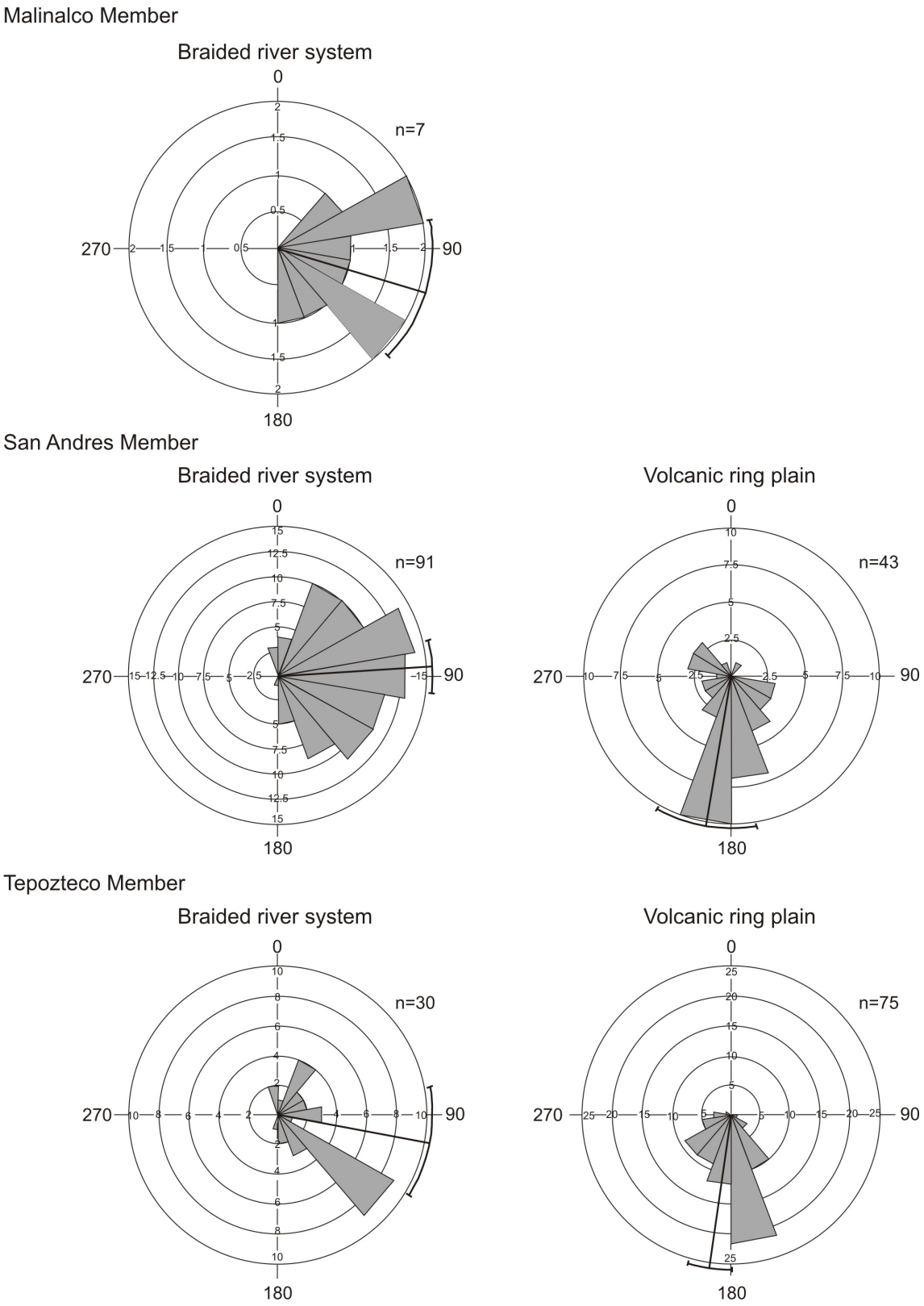

Figure 5. Paleocurrent directions within the three Members of the Tepoztlán Formation measured from primary sedimentary structures, i.e. trough cross-stratification, asymmetric ripple marks and the shape of scours and channels in sandstones and conglomerates.

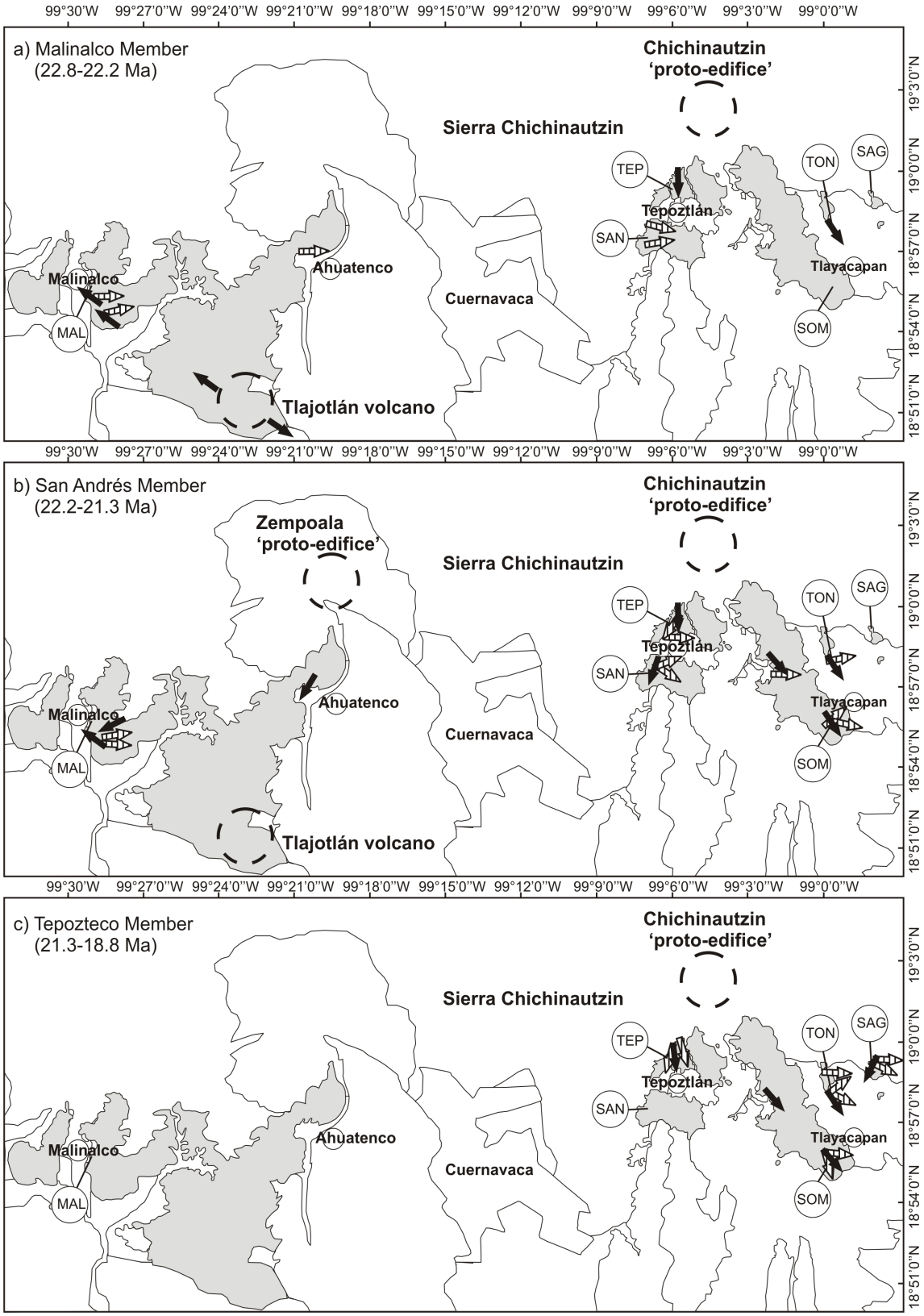

Figure 6. Paleocurrent directions of the three Members of the Tepoztlán Formation inferred from AMS analysis (black arrows) and sedimentary features (dashed arrows) showing proposed river flow directions and volcanic source areas. The grey areas show the modern-day distribution of the Tepoztlán Formation. Discontinuous circles represent proposed volcanic edifices.

Tables:

Table 1. Mean values of magnetic susceptibility data collected for each site. LF = Lithofacies: La = lava; Tu = tuff; Tb = tuffaceous breccia; Co = conglomerate; Sa = sandstone. *n* = number of specimens measured. AMS parameters are defined in the text.

Sites	LF	*n*	*K*m (10^{-4} SI)	*K*1 mean	*K*2 mean	*K*3 mean	α95 *K*1	α95 *K*2	α95 *K*3	AMS parameters			
										L	*F*	P_j	*T*
TL 1	Tb	5	6.80	69/24	320/36	185/44	18	13	18	1.008	1.022	1.033	0.295
TL 2	Tu	5	9.74	280/13	12/8	132/75	8	10	8	1.012	1.025	1.038	0.330
TL 4	Tu	5	5.76	13/6	282/11	131/77	19	11	12	1.011	1.024	1.036	0.359
TL 5	Tu	5	7.45	328/24	63/10	174/63	7	7	6	1.013	1.011	1.025	-0.062
TL 7	Tu	6	9.10	289/20	20/4	120/69	6	13	6	1.024	1.028	1.053	0.043
TL 8	Tu	5	10.1	263/37	13/25	129/43	4	19	5	1.005	1.007	1.012	0.202
TL 9	Tu	5	7.47	329/13	59/1	154/77	6	9	9	1.005	1.004	1.009	-0.178
TL 10	Sa	7	12.6	346/24	77/3	174/65	18	13	20	1.005	1.005	1.010	0.042
TL 11	La	8	3.15	275/19	11/19	143/63	10	6	8	1.018	1.026	1.046	0.213
TL 12	La	9	5.92	59/31	258/56	154/9	9	9	6	1.014	1.047	1.065	0.556
TL 13	Co	5	69.1	40/29	234/60	133/6	9	8	7	1.010	1.011	1.021	0.211
TL 14	Sa	5	51.6	351/13	86/11	214/73	14	14	5	1.004	1.008	1.012	0.326
SO 1	La	10	5.68	272/29	181/1	89/61	13	20	12	1.013	1.050	1.069	0.572
SO 2	Tu	10	5.66	203/0	293/5	112/85	22	19	21	1.009	1.016	1.026	0.284
SO 3	Tu	8	2.49	59/14	150/1	245/75	7	8	7	1.012	1.019	1.031	0.282
SO 6	La	7	1.76	199/7	295/42	102/47	4	13	3	1.023	1.106	1.141	0.642
SAC	La	10	26.3	13/29	279/7	177/60	4	7	6	1.006	1.032	1.041	0.667
SA 4	Tu	5	47.8	281/34	59/48	176/22	15	12	16	1.012	1.014	1.026	-0.043
SA 5	Tu	5	63.8	7/36	240/39	122/30	11	12	12	1.019	1.030	1.050	0.216
SA 6	Tb	8	66.3	349/34	239/28	118/44	14	12	11	1.013	1.030	1.045	0.413
SA 7	Tu	5	59.2	157/2	247/9	52/81	4	17	4	1.007	1.029	1.039	0.627
SA 8	Tu	5	67.0	233/24	345/41	121/40	9	14	10	1.003	1.007	1.010	0.301
SA 10	Tu	5	51.3	320/22	51/4	150/68	3	16	4	1.004	1.011	1.015	0.471
SA 11	Tu	5	52.1	174/0	264/39	83/51	3	21	7	1.006	1.013	1.019	0.389
SA 13	Tu	5	64.3	13/62	263/10	168/25	21	12	7	1.007	1.016	1.024	0.366
SA 15	Tu	5	65.8	340/37	94/28	211/40	4	8	13	1.015	1.026	1.042	0.257
SA 16	Tu	5	20.9	293/60	195/5	102/30	10	2	3	1.008	1.018	1.028	0.398
SA 18	Tu	6	51.3	293/42	197/7	99/47	6	9	6	1.006	1.012	1.019	0.374
SA 19	Tu	5	37.1	237/38	341/17	89/47	19	11	11	1.007	1.011	1.019	0.259
SA 20	Tu	6	38.8	94/63	315/21	219/16	25	14	15	1.004	1.009	1.013	0.484
SA 21	Tu	5	55.9	309/11	217/9	91/75	15	8	8	1.006	1.012	1.019	0.317
SA 23	Co	5	57.2	325/23	232/9	122/65	7	6	4	1.023	1.051	1.078	0.358
SA 24	Co	5	67.1	310/13	44/16	183/69	15	11	13	1.004	1.010	1.015	0.320
SA 25	Co	6	50.1	63/4	333/3	203/85	6	6	3	1.002	1.007	1.009	0.515
SA 26	Sa	5	49.2	244/21	334/0	66/68	5	14	5	1.002	1.002	1.004	-0.008
TPO	Sa	7	50.1	320/18	230/0	138/72	8	10	9	1.005	1.011	1.017	0.280
TE 9	La	8	7.03	117/29	207/0	298/61	9	22	12	1.012	1.010	1.023	-0.044
TE 10	La	8	7.30	325/64	160/25	67/6	8	9	8	1.013	1.014	1.028	0.072

TE 11	La	7	4.64	50/8	315/30	154/59	5	6	5	1.010	1.012	1.023	0.156
TE 12	Sa	8	6.86	135/6	43/20	241/69	16	19	26	1.005	1.009	1.015	0.306
MA 1	Tu	11	4.49	106/2	196/8	3/82	8	21	7	1.006	1.009	1.016	0.151
MA 2	Tu	11	6.14	159/5	68/11	272/78	8	26	7	1.005	1.006	1.011	0.003
MA 3	Tu	21	5.89	48/12	317/5	206/77	7	6	6	1.006	1.019	1.027	0.300
MA 4	Sa	21	9.58	121/17	212/2	308/73	17	9	10	1.005	1.007	1.013	0.347
MA 5	Sa	6	4.48	325/12	56/6	173/77	7	14	8	1.006	1.009	1.015	0.152
MA 6	Tu	5	7.66	73/5	343/1	242/85	8	10	3	1.005	1.011	1.017	0.384
MA 7	Sa	12	6.88	351/12	259/7	140/76	8	8	8	1.018	1.054	1.076	0.467

Table 2. Paleocurrent directions from clastic strata of the Tepoztlán Formation

Member (depositional setting)	n	Mean direction	Standard Deviation	95% Confidence Interval
Malinalco (braided river)	9	106°	35.5°	79.3° - 134.6°
San Andres (braided river)	91	85°	48.6°	76.5° - 96.4°
San Andres (volcanic ring plain)	43	186°	60.5°	170.4° - 208.7°
Tepozteco (braided river)	30	116°	57.3°	79.4° - 122.0°
Tepozteco (volcanic ring plain)	75	181°	36.7°	179.8° - 196.3°